RESEARCH

Temporal Defocusing as a Depth Diagnostic of Submerged Sources of Transient Acoustic Emission from Solar Flares

Savannah Perez-Piel[1] · Juan Camilo Buitrago-Casas[1] · Juan Carlos Martínez Oliveros[1] · Charles Lindsey[2]

Abstract

Helioseismic holography applied to HMI observations of a sunquake associated with the SOL20140207T10:29M1.9 flare hosted by NOAA AR11968 shows the signature of a compact submerged acoustic source. In the $9-11$-mHz bandpass, this source appears to be at a depth of 2 Mm. This is nearly double the depth of the highly impulsive acoustic transient, referred to as an ultra-impulsive transient source recently found in the SOL20110730T02:09M9.3 flare, emerging from NOAA AR11261 in 2011. The latter source was compound, having multiple surface components overlaying a single submerged component. Many of the sources observed have evidence of being constituted of multiple components, some of which are staggered in depth. The helioseismic source of the flare of 2014-02-07 is distinguished by the apparent *absence* of a strong shallow compact overlying source component matching the character of those apparent in the flare of 2011-07-30. This suggests that the volume several Mm beneath active-region photospheres could possibly harbor many more ultra-impulsive transient acoustic sources than the rarities that have so far appeared in familiar surface-focal-plane diagnostics. Based on weak surface signatures that appear in place of the strong ones, we find a temporal delay between weak surface and strong submerged sources similar to that found between surface-and-submerged sources in the flare of 2011-07-30. While it remains highly speculative based on the limited statistics we have at this point, this temporal delay supports a model in which the submerged source is perturbed by some presently invisible triggering disturbance that propagates downward from the flaring outer atmosphere at ~ 5 km s^{-1}. This is slower than the sound speed anywhere in the $0-2$-Mm depth range. However, this potentially could be an Alfvèn speed if submerged magnetic flux densities along which the trigger propagates are as high as possible. The standard local-helioseismic diagnostics we have used in the past have been heavily reinforced in this study by a powerful new control resource found in the recognition of *temporal defocusing* of compact transient sources. In particular, its tight relationship to the standard spatial defocusing upon which helioseismic holography has capitalized from its early advent.

Keywords Flares · Helioseismology

1. Introduction

Sunquakes are a photospheric manifestation of seismic energy released into the solar interior during the impulsive phases of some flares. It has long been our general understanding that

energy released by the flare during its impulsive phase somehow drives an acoustic transient into the subphotosphere of the flaring region. The high sound-speed gradient in the acoustic medium underlying the photosphere refracts most of the induced waves back to the overlying surface within about 50 Mm of the source in the succeeding half hour or so. "Sunquake" refers to the surface disturbances that result when the returning transient impinges back upward into the photosphere surrounding the flaring region. Seismic emission from flares was predicted in 1972 by Wolff and first observed from the flare of 1996 July 9 by the Solar and Heliospheric Observatory (SOHO) (Zharkova and Kosovichev, 1998; Kosovichev and Zharkova, 1998).

The scientific context of this study is a model whereby some mechanism affects the release of some cache of free energy from a compact region in the solar medium in the form of an acoustic transient that propagates coherently downward from the release site to be refracted back to the surface. The direct helioseismic manifestation of this transient are ripples propagating outward along the solar surface from the release site (Martínez et al., 2020). Our helioseismic diagnostic computationally extrapolates this propagation backward in time from the surface ripples to the source region up to the moment we propose the energy released became acoustic in nature.

The application of *computational helioseismic holography* (e.g., Lindsey and Braun, 1997) to sunquake ripples (Donea, Braun, and Lindsey, 1999; Donea and Lindsey, 2005) has told us much about the sunquake phenomenon. This diagnostic gives us detailed images of the source distributions of acoustic transients, which can be spatially related to flare phenomena in the overlying outer atmosphere of the flaring region. Such a source can be identified with its spatial distribution mapped with the techniques of helioseismic holography.

The most persistent mystery with which these diagnostics have confronted us has been indications of strong acoustic sources that are locally devoid of matching transient phenomena in the outer flaring atmosphere. Even so much as a plain Doppler disturbance horizontally cospatial with the acoustic sources extrapolated by seismic holography is unseen in these cases. These instances are hard to reconcile with acoustic emission driven directly by coronal magnetic energy released in the *outer* atmosphere. The question arises, how does the driving mechanism inject an intense, compact acoustic disturbance *through* the photosphere and into the underlying interior without acoustically disturbing the local photosphere through which it passed? This lack of a local photospheric disturbance suggests a *submerged* source of transient acoustic emission, possibly with its own accumulated energy supply. This stored energy could then be *triggered* by a relatively weak impetus released through a compact locality into the active-region subphotosphere by the overlying solar flare, an impetus that needs to be neither compact nor visible to our helioseismic diagnostics.

This opens a new question of how an acoustic driver submerged less than a megameter – the estimated depth discrimination of standard seismic holography – might contrive to release a strong acoustic transient downward into the solar interior in such a way that would leave the overlying surface undisturbed. On the other hand, the heavy suppression of the response of strong-magnetic photospheres to upwardly propagating p-modes (see, e.g., Braun, 1995; Braun and Lindsey, 2000; Cally, 2000; Donea and Lindsey, 2005; Schunker et al., 2005) ought to apply equally, we propose, to a transient propagating directly upward from an emitter submerged beneath a flaring region.

The advent of ultra-impulsive transient helioseismology (Zharkov et al., 2011, 2013) has recently opened flare seismology to unprecedented spatial resolution, both horizontally and in-depth, by virtue of the $9-11$-mHz spectrum. Martínez et al. (2020) and Lindsey et al. (2020) found a 10-mHz source component in the flare of 2011-07-30 from NOAA

AR11261 that comes into sharp focus a full megameter beneath its overlying penumbral photosphere, strongly supporting the hypothesis of submerged transient acoustic sources. A great deal of what has been proposed by Lindsey et al. (2020) remains highly speculative, even if the depth diagnostics are secure. In any case, depth diagnostics are now crucial in opening a broad new domain of avenues to be explored in the mechanics of transient acoustic emission from flares – and its possible implications for the magnetic environments beneath active-region photospheres.

The subject of this study then is the depth diagnostics that are now lending support to the hypothesis of submerged acoustic transients. In some respects, indications that acoustic sources with no horizontally cospatial disturbances in the outer atmosphere are submerged, are controlled by the apparent *need* for submergence based on the preceding considerations going back long before helioseismic holography indicated any but shallow sources. This study considers a second control resource alternative to the standard focus–defocus diagnostics, on which helioseismic holography has traditionally capitalized. This diagnostic avenue recognizes a *temporal defocusing*, i.e., spreading of the *temporal* profile of the seismic signature, closely related to the spatial defocusing applied by Lindsey et al. (2020). This diagnostic crowbar is a natural result of an intimate relationship between the temporal and spatial dependencies of the acoustic field in media that confer the diagnostic benefits of wave mechanics.

We illustrate temporal defocusing by applying it comparatively with standard spatial defocusing in two instances. The first is an evidently relatively shallow acoustic source from an M9.3-class flare on 2011-07-30; the second appears to emanate from some at the depth of 2 Mm beneath the quiet photosphere during an M1.9-class flare on 2014-02-07.

## 1.1. Data Resources

1.1.1. Survey

This study draws from a survey of 18 sunquakes examined by Buitrago-Casas et al. (2015), all occurring in Solar Cycle 24.

1.1.2. Instruments

We use helioseismic Dopplergrams, line-of-sight magnetograms, and visible-continuum data of the Sun observed by the Helioseismic and Magnetic Imager (HMI; Scherrer et al., 2012) aboard NASA Solar Dynamics Observatory (SDO; Pesnell, Thompson, and Chamberlin, 2012). The SDO spacecraft was launched in 2010 with HMI onboard (one of three instruments) to record Dopplergrams, continuum filtergrams, and line-of-sight and vector magnetograms. It remains in operation at this writing. The acoustic source-density maps in Figures 3 and 4 are derived from HMI Dopplergrams. The project also uses EUV observations from the Atmospheric Imaging Assembly (AIA) (Lemen et al., 2012) likewise aboard the SDO.

While NASA Reuven Ramaty High Energy Solar Spectroscopic Imager (Lin et al., 2002) observed HXR emission from all of these flares, and this was used as a selection criterion in a previous study (Buitrago-Casas et al., 2015), these observations are not otherwise incorporated into this study.

Figure 1 The Sun in EUV (He II 304 Å) on 2011-07-30, shortly before onset of the flare of 2011-07-30. NOAA AR11261, from which the flare emanated, is marked by an enclosing yellow circle in the northeastern (upper-left) hemisphere. The dashed circle, 100 arcsecs inside of the limb, marks the region in which ultra-impulsive transient helioseismic holography can be applied.
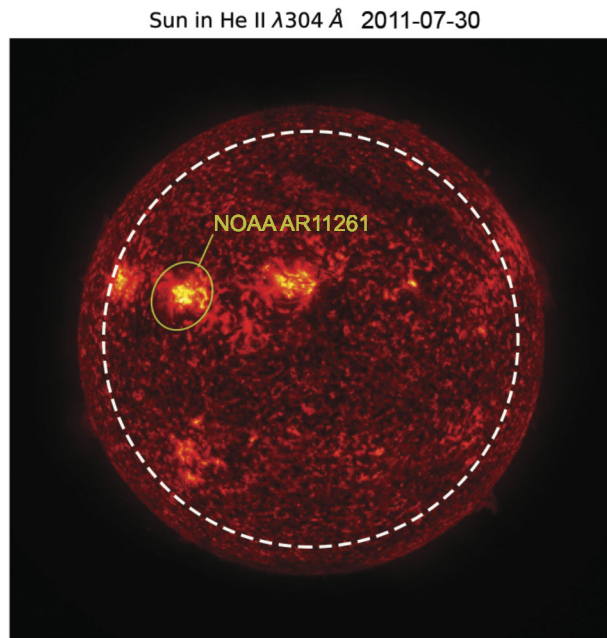
2. Techniques and Analysis

We will begin our discussion of techniques and analysis by illustrating their application to observations of the M9.3 class flare of SOL20110730T02:09, examining an associated compact acoustic source that had no sign of significant submergence.

2.1. Flare of 2011-07-30

Figure 1 shows the location of AR11261 a few minutes before the onset of the M9.3 class flare, whose onset was at 02:04 UTC. The flare released a strong acoustic transient with shallow sources on sharp magnetic boundaries, described by Martínez et al. (2020), and a submerged source described by Lindsey et al. (2020). The subject of this section is one of the shallow acoustic sources that appear in this flare, to be compared, then, with a considerably submerged source that appears in another flare.

In Figure 2, we display the GOES $12-25$ keV X-ray flux in red and AIA 1700-Å intensity in blue. GOES provides global, nonlocalized measurements of X-ray flux, and from AIA we plot only the EUV (1700-Å) flux from the flaring active region. These light-curves certify the occurrence of a flare and fix its onset at 2:04 UTC.

We proceed with a summary of the depth diagnostics employed, first applying them to the foregoing relatively shallow acoustic source we have selected as our control subject.

2.2. Computational Helioseismic Holography

This study is based upon the application of computational helioseismic holography (Roddier, 1975; Braun et al., 1992; Lindsey and Braun, 1997; Braun et al., 1998; Lindsey and Braun, 2000) to 10-mHz – specifically the $9-11$-mHz bandpass – helioseismic observations of surface Doppler ripples seen traveling outward along the solar surface from the flaring region
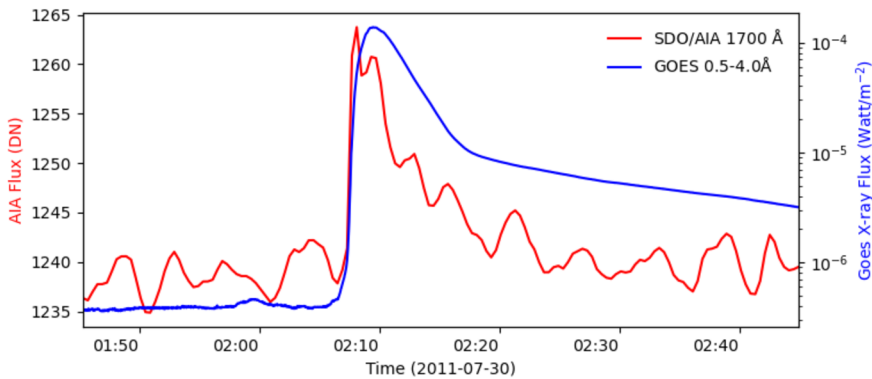
Figure 2 The GOES 12-25 keV X-ray flux in red and AIA 1700 Å intensity in blue, depicting the flare and its onset at 2:04 UTC.

up to an hour following its onset. This diagnostic is based on recognition that the observed ripples are surface disturbances due to waves emitted downward into the solar interior during the flare's impulsive phase and eventually being refracted back upward into the surface. Computational helioseismic holography applies standard wave mechanics in time reverse to the surface disturbances, coherently extrapolating them back in time, back down into the solar interior, and from thence back up to the source region.

We regard both the surface ripples and extrapolated acoustic source density to be acoustic signatures of the source. For an illustration of the former, we refer to Kosovichev and Zharkova (1998). In this study, we illustrate only the latter.

This phase-coherent extrapolation delivers diffraction-limited maps of the *acoustic source-power density*, $|H_+|^2$ – from hence just "source-density" – over the region so represented. If a compact source lies on the sampling surface, then it is rendered in sharp focus. As the sampling surface is moved above or below the source depth, the source signature becomes diffuse, i.e., out of focus, and hence "weakened." From here we refer to the sampling surface by its familiar optical counterpart, "focal plane".

The forgoing "focus–defocus" profile can tell us a lot about the depth of a compact source. We first aim to illustrate this diagnostic applied to our control subject, the 10-mHz source density of which is mapped in the bottom right frame of Figure 3. The compact signature we identify as our control source is at the center of the blue circle (radius 8.3 Mm). At the outset, it shows strong circumstantial evidence of having a relatively shallow compact component in close horizontal proximity to a compact site of intense 10-mHz photospheric oscillations, whose mean square amplitude ("local acoustic power") is mapped in the bottom-left frame. Other transient phenomena in the outer atmosphere are cospatially mapped in the overlying middle row.

Specifically, the other panels in Figure 3 show, cospatially, the preflare continuum intensity (top left), the preflare line-of-sight magnetic field (top right), and other surface manifestations of a photospheric disturbance during the directly succeeding impulsive phase of the flare. The middle-left panel, for instance, shows the transient variation in continuum intensity in the impulsive phase of the flare. The middle-right panel maps the EUV (He II λ304 Å) intensity at flare maximum. The lower-left panel shows the local square variation in $9-11$-mHz Doppler oscillations concurrent with the source distribution mapped in the lower-right frame.
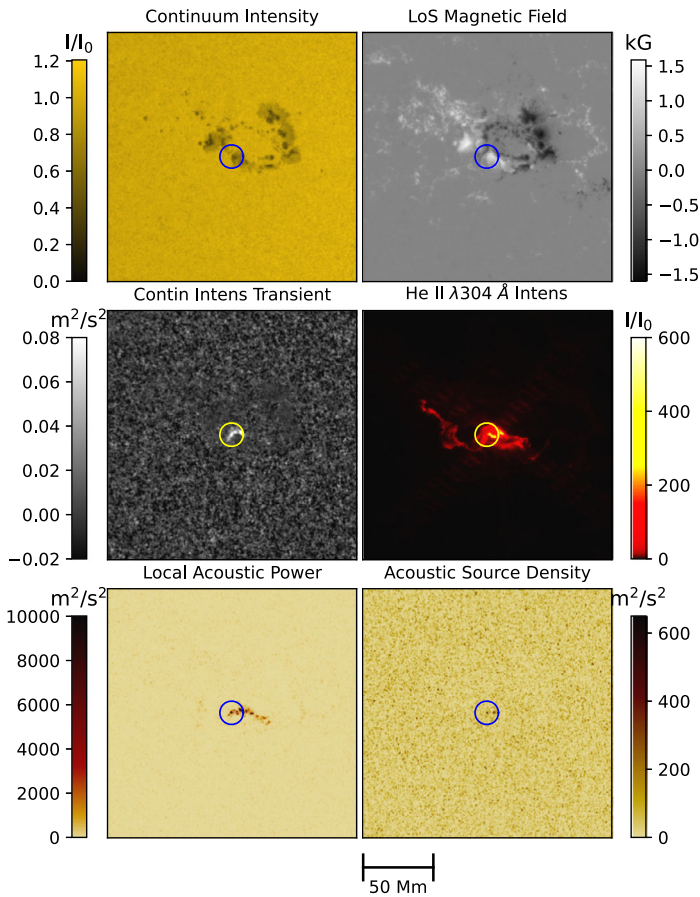
Figure 3 Sources of 9–11-mHz acoustic emission from NOAA AR11261 during the impulsive phase of SOL20110730T:02:04 are imaged (bottom right) cospatially with preflare continuum intensity (upper-left), preflare line-of-sight magnetic field (upper-right), transient increase in continuum intensity in the impulsive phase of the flare (middle-left), EUV intensity (middle-right) in the line He II λ304 Å, during the impulsive phase of the flare, and mean-square amplitude of local acoustic oscillations in the 9–11-mHz spectral band during the impulsive phase (lower-left).

2.3. Criteria for Attribution of Helioseismic Signatures to Flare Mechanics

The quiet Sun is constantly generating acoustic noise. This is everywhere evident in the source density mapped in the lower-right panel of Figure 3, showing the ubiquitous manifestation of thousands of individual compact, contiguous sources throughout the quiet Sun outside of the flaring region. Together, these manifest a positive mean source density of 39.81 m^2 s^{-2}. Our judgment that the control source is sufficiently significant to attribute it to a nearby flare is, admittedly, somewhat rough and subjective. It is based on an assessment of the probability that a signature of the magnitude of one which we propose to attribute to anomalous mechanics, such as that driving a flare, can be expected to occur by accident in nominal (nonflaring) mechanics.

To make this assessment, we formulate a one-dimensional array of evenly spaced source density values, each of which is given the role of a threshold, $|H_+^t|^2$, up to a maximum of
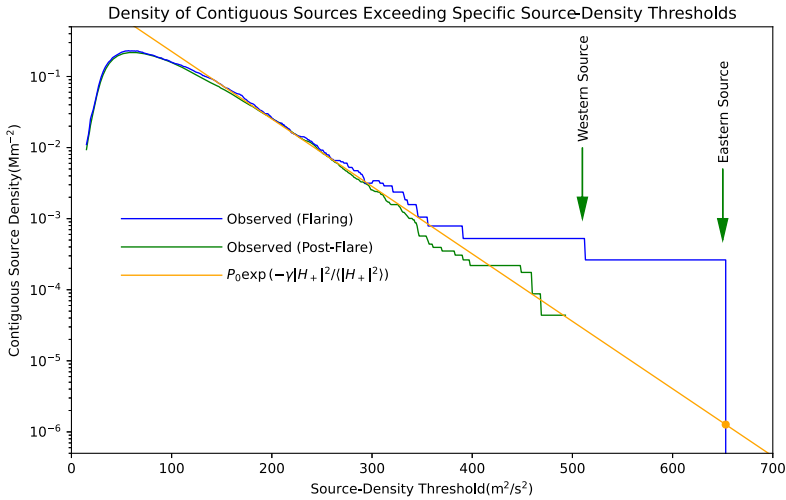
Figure 4 Plot of the density P_{cs} of contiguous source regions within 35 Mm of the blue circle plotted in all of the frames in Figure 3 that exceed source-density thresholds up to 700 m^2 s^{-2}. The blue curve plots P_{cs}, the number of contiguous sources that appear in the lower-left panel of Figure 3, i.e., at acoustic source maximum during the impulsive phase of the flare. The Green curve plots the P_{cs} averaged over the hour succeeding acoustic maximum. The amber curve plots the exponential fit to the blue curve specified by Equation 1.

700 m^2 s^{-2}. For each of these thresholds, we compose a mask cospatial with the frames in Figure 3 that admits all points at which the source density $|H_+|^2$, mapped in the lower-right frame of Figure 3, *exceeds* $|H_+^t|^2$, assigning unity to all pixels that exceed $|H_+^t|^2$ and zero to those that do not. To each of these maps, we apply an algorithm that discriminates each region that is *spatially contiguous* and counts all of these contiguities that lie within a circle 35 Mm in radius about the control source. These counts are divided by the area of the 35-Mm circle, some 3850 Mm^2, to deliver a *contiguous source density* P_{cs} and hence a number of contiguous sources per Mm^2. Figure 4 plots $P_{cs}(|H_+^t|^2)$ in bright blue for values of its argument up to 700 m^2 s^{-2}. For thresholds ranging from 150 to 400 Mm, the contiguous source density $P(|H_+^t|^2)$ conforms tightly to a profile of the form

$$P(|H_+^t|^2) = P_0 e^{-\gamma|H_+|^2/\langle|H_+|^2\rangle}, \tag{1}$$

where the mean value $\langle|H_+|^2\rangle$ of the source density over the foregoing region is 39.81 m^2 s^{-2}, γ is 0.870, and P_0 is 2.00 Mm^{-2}.

For high thresholds, the distribution of sources whose maxima exceed them is spatially sparse, and P_{cs} appears to conform to a decaying exponential (amber locus) as it would to the power (square modulus) of an undersampled complex Gaussian random variable (Donea, Lindsey, and Braun, 2000). As the threshold decreases toward lower values, and P_{cs} approaches densities comparable to the reciprocal of the spatial resolution, neighboring contiguities touch each other and fuse; P_{cs} then turns over and decreases precipitously, characterizing a field of densely packed contiguities that are massive and now numerically sparse. Our interest is in the sparse, compact contiguities with *high* maximum source densities, which fit nicely to the exponential represented by the amber locus. The acoustically brightest two sources depart considerably to the right of this asymptote. The most intense is the one on which the blue circle is centered in the bottom right frame of Figure 3. It has
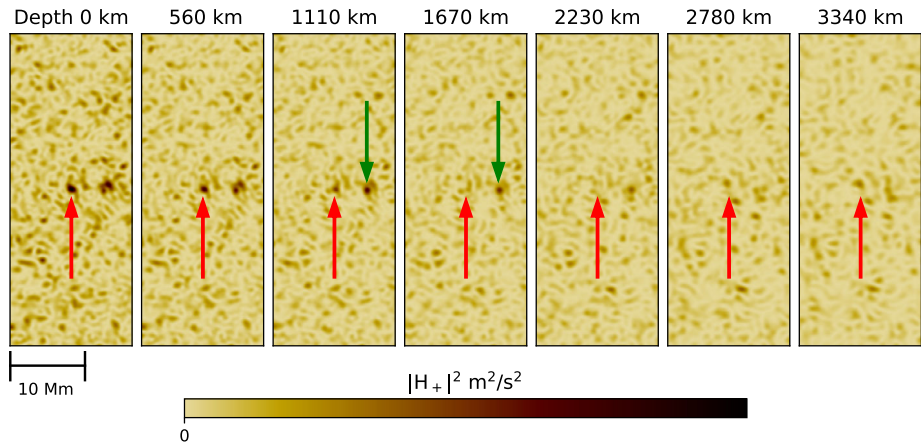
Figure 5 Sequence of acoustic source-density maps with the focal plane successively submerged from the level of the quiet photosphere (far left) to a depth of 3340 km thereunder (far right). The red arrow in each frame horizontally locates an apparently relatively superficial source. The green arrows in the third and fourth frames horizontally locate a source thought to be submerged to an approximate depth of 1150 km.

a maximum source density of 653 $\mathrm{m^2\,s^{-2}}$. The expectation density of contiguous sources reaching (or exceeding) this value is (amber dot near the lower-right corner of the plot) 1.3×10^{-6} $\mathrm{Mm^{-2}}$. The area A of the blue circle (radius 8.3 Mm) is 220 $\mathrm{Mm^2}$. Over a full solar hemisphere ($A = 3 \times 10^6$ $\mathrm{Mm^2}$), we should expect to see something like $P_{cs}A = 4$ acoustic signatures like the one in the center of the blue circle in the lower-right frame of Figure 3 by accident as a manifestation of standard Gaussian statistics even if there is no real acoustic anomaly at work. The probability of one of these sources appearing within the blue circle in a field of random Gaussian noise is only $P_{cs}A = 2.8 \times 10^{-4}$, hence the likely association of the signature to extra-Gaussian flare mechanics in the general neighborhood of the blue circle, in our assessment.

2.4. Signature of a Shallow Compact Acoustic Source in a Submerged Focal Plane

The existence of a sharp, compact source in the center of the blue circle in the lower-right frame of Figure 3 does not preclude a further underlying submerged source. Furthermore, many strong surface manifestations of the flaring outer atmosphere exist in regions from which no significant transient emission emanates. Figure 5 takes us through the exercise of applying computational seismic holography to 9 – 11-mHz source distributions in sampling surfaces, i.e., "focal planes," ranging from the surface to an eventual depth of 3340 km. The signature is of the compact source located in each frame by the red arrow is sharpest where the focal plane is shallow and quickly fades to obscurity as the focal plane descends. The 560-km separation in focal-plane depths is chosen to slightly overample our helioseismic diagnostics $\pm$ 400 km resolution.

For comparison, the green arrows in the third and fourth frames point to a signature that becomes sharp between 1110 and 1670 km beneath the photosphere before fading to obscurity. These are the subject of Lindsey et al. (2020), who propose to attribute this signature to a source submerged approximately 1150 km beneath the photosphere.

Figure 6 Temporal profile of the source density for the 2011-07-30 sunquake over focal-plane depths ranging from 0 to 2.92 Mm. Green locus plots the source density as a function of time for a focal-plane fixed at the base of the quiet photosphere, i.e., depth 0. Red locus plots the same over a focal-plane submerged 2000 km beneath the surface. The grey vertical line notes the onset of the flare, as defined by GOES. The I-bar at the top left shows the temporal resolution specified by Equation 2.
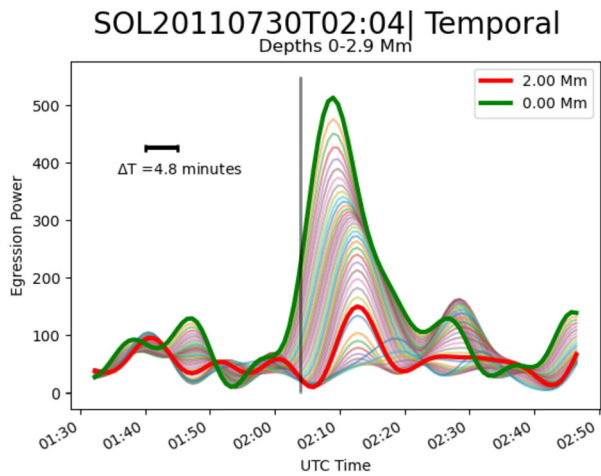
2.5. A New Depth Diagnostic

We now turn our attention to a quality of acoustic signatures that is closely related to their spatial profiles, i.e., their *temporal* profiles. The source density projected to any focal-plane depth depends on both time and horizontal location in the focal plane. Integrated over a region completely enclosing the spatial extent of the signature, we might guess that the result would be independent of focal plane depth as the Green function is unitary. However, when the focal plane is raised or lowered above or beneath the source depth, the signature is not only defocused spatially; its coherence is impaired by different components from different locations in the pupil arriving into whatever their shifted destinations in the focal plane at the "wrong time," weakening it so as to shift power to *other times* in its profile.

Suppose the signature is integrated over both space *and* time. In that case, the result should be independent of focal plane depth as long as the region over which the signature is spatially integrated completely encloses the defocused profile and the time interval over which the integral is computed securely encompasses the full duration of the temporally spread-out signature.

From the outset it appears that there must be some similarities between the dependence of the spatial and temporal profiles on focal-plane depth. For example, they must share the same maximum, and this must occur in the same location, including the same depth. The experiment we now pursue is to examine in what other ways the spatial profile reflects the temporal.

Figure 6 plots the temporal profile of the $9-11$-mHz source density of the sunquake related to the flare of 2011-07-30 at 2:04 UTC integrated over a circle of radius 1.4 Mm enclosing the source location at a range of depths. The sharply peaked green locus identifies the temporal profile when the focal plane is located at the surface.

We understand that the temporal discrimination of helioseismic signatures is fundamentally limited to the reciprocal of the width $\Delta\nu$ of the spectrum of the oscillations admitted into the pupil of the seismic extrapolation being computed. In this study, this is compressed to within 2 mHz of the Nyquist frequency of the HMI observations to eliminate the overwhelming confluence of lower-frequency emission for which the diffraction limit is too

Figure 7 Time-Depth plot for the 2011-07-30 sunquake in the 9 – 11-mHz spectrum, with source density rendered in color and the *y*-axis indicating focal-plane depth. Horizontal fiducial marks 2-Mm depth. Flare onset is at 2:04 UTC.
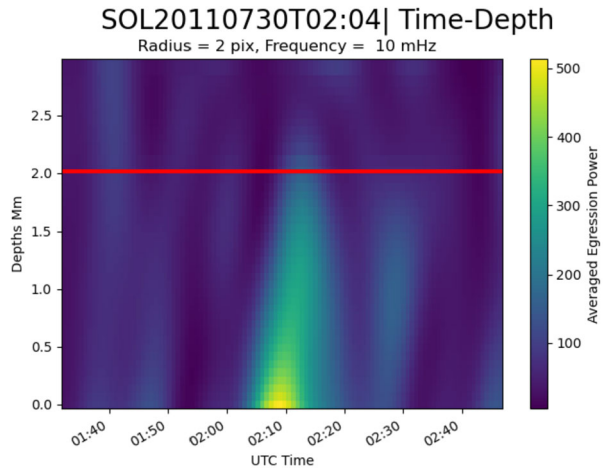
coarse for the depth discrimination needed to resolve the issue at hand. Hence

$$\Delta t = \frac{1}{\Delta \nu} = \frac{1}{0.002 \text{ Hz}} = 500 \text{ sec} = 4.8 \text{ min.} \tag{2}$$

This interval is marked on the temporal plots and is seen to approximately match the width of the Gaussian related to the onset of the flare at 2:04 UTC, marked by the green locus displaying the surface source density in Figure 5.

The red locus in the plot identifies the source profile when the focal plane is at a depth of 2.0 Mm. The temporal profile is clearly seen to spread and weaken as the focal plane is submerged beneath the surface. Temporal defocusing condenses the 3D presentation of spatial defocusing of the horizontal extent of the source signature as a function of depth to a simple planar image of temporal extent as a function of depth.

Figure 7 shows the profiles plotted in Figure 6, now using color to signify the source density so that the vertical axis can be appropriated to represent focal-plane depth. This comet-like rendering shows the same spreading/weakening as the focal plane submerges beneath the surface. In addition, this "comet" shows a conspicuous *tilt* from verticality, which is also evident in Figure 6. In this instance, the tilt of the "comet" is not the signature of any seismic emission beneath the surface, as there apparently is none. It is rather simply a signature of the mean sound speed 11.2 km s^{-1} of the medium composing the solar model (Model S of Christensen-Dalsgaard, Proffitt, and Thompson, 1993), as incorporated into the Green function that prescribes our holographic extrapolations of the sunquake ripples into the solar interior and thence back up to focal planes distributed over a range of depths. Figures 7 and 13 show the actual focal-plane depths of the acoustic intensities plotted in Figures 6 and 12, respectively. Here the *x*- and *y*-values are geometric displacements in standard distance units with the acoustic intensities represented by color in place of displacement in *y*. This facilitates slope estimates, for example, which express vertical velocities.

2.6. Flare of 2014-02-07

We now arrive at the primary subject of our study, an acoustic source that appears to be considerably submerged beneath the photosphere. Of some 18 sunquakes included in Buitrago-Casas et al. (2015), the flare that released this transient was a relatively weak one, class

Figure 8 The Sun in EUV (He II 304 Å) at 10:26:00 UTC on 2014-02-07 about five minutes before onset of the M1.9-class flare of 2014-02-07. NOAA AR11968, from which the flare emanated, is circled in amber and annotated. The dashed circle, 100 arcsecs inside of the limb, marks the region in which ultra-impulsive transient helioseismic holography can be applied.

Sun in He II λ304 Å 2014-02-07

NOAA AR11968
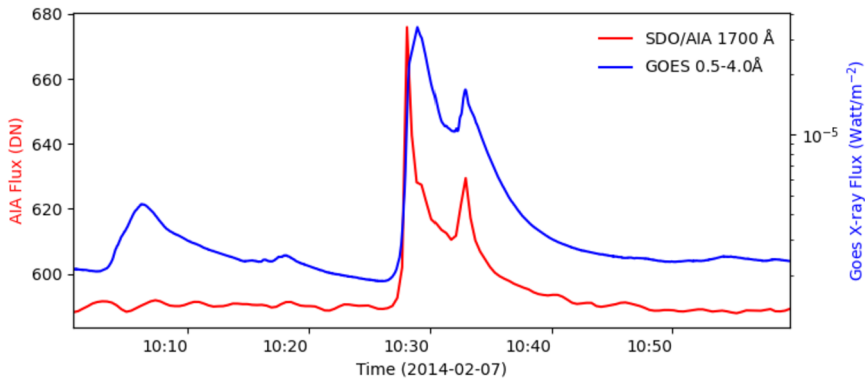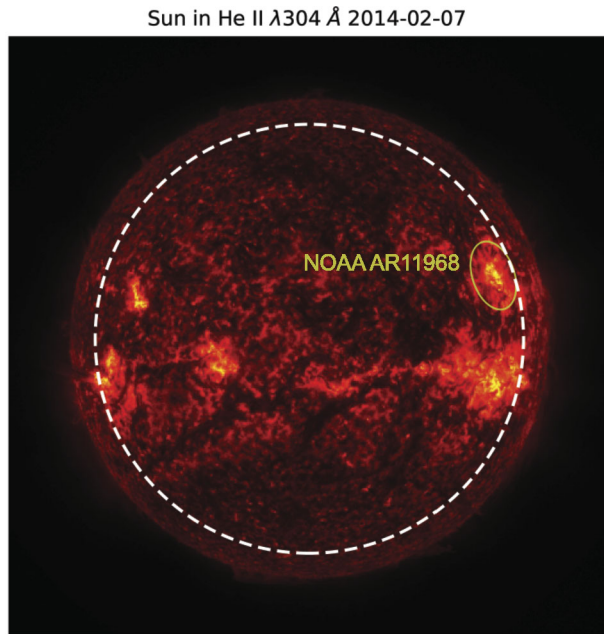
Figure 9 GOES 12-25 keV X-ray flux in red and AIA 1700 Å intensity in blue for the flare of 2014-02-07 at 10:28 UTC. Two peaks are seen in each curve and are respectively related to two distinct energetic releases that occurred in sequence within NOAA AR11968.

M1.9, emanating from NOAA AR11968 (Figure 8). The flare began at 10:25 UTC on 2014-02-07, reaching a maximum EUV (He II 304 Å) irradiance five minutes thenceforth and fading back to relative EUV obscurity about 30 minutes thereafter by about 10:54 UTC (Figure 9).

Figure 10 shows a mosaic of cospatial frames comparing preflare continuum intensity (upper-left) and line-of-sight magnetic field (upper-right) with local acoustic power in $9-11$-mHz oscillations (middle-left), EUV intensity (middle-right), and acoustic source densities in $5-7$-mHz emission (lower-left) and $9-11$-mHz emission (lower-right) focused at the surface during the impulsive phase of the flare. The magnetic classification is β-γ,
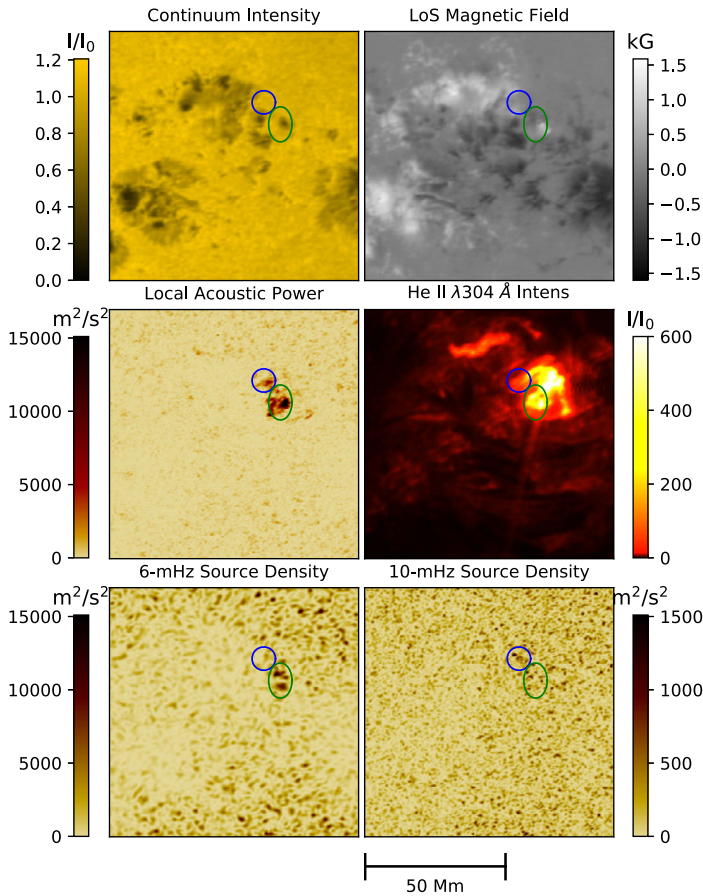
Figure 10 Sources of acoustic emission from NOAA AR11968 during the impulsive phase of SOL20140207T10:2 are imaged (bottom row) cospatially with preflare continuum intensity (upper-left), preflare line-of-sight magnetic induction (upper-right), mean-square amplitude of local acoustic oscillations in the $9-11$-mHz spectral band during the impulsive phase (middle-left), and EUV intensity (middle-right) in the line He II $\lambda304$ Å during the impulsive phase of the flare. The bottom-left panel shows a map of acoustic source density in the $5-7$-mHz band during the impulsive phase of the flare focused at the base of the quiet photosphere. The bottom-right panel shows the same for $9-11$-mHz emission.

designating a bipolar group with a complex magnetic-polarity configuration. Regions with conspicuous acoustic signatures closely associated with each other in this figure are circled in blue. The primary subject of this section will be helioseismic signatures that appear in the upper, northernmost circle (8.3-Mm radius) in all of the frames of Figure 10.

Although a conspicuous compact signature of intense local $9-11$-mHz oscillations appears in the lower-right of the upper circle of the middle-left frame of Figure 10, signatures of helioseismic emission from this region (bottom row of Figure 10) are not especially conspicuous ($P_{cs}A = 0.063$). This changes radically as the focal plane is submerged. Figure 11 shows the source density over focal planes ranging from Depth 0 (far left) to 3340 km (far right). The red arrow in each frame points to a region in which the source density collapses to a single sharp, compact condensation in the fourth and fifth frames, in focal planes 1670 and 2230 km, respectively, beneath the base of the quiet photosphere, and in the deeper of
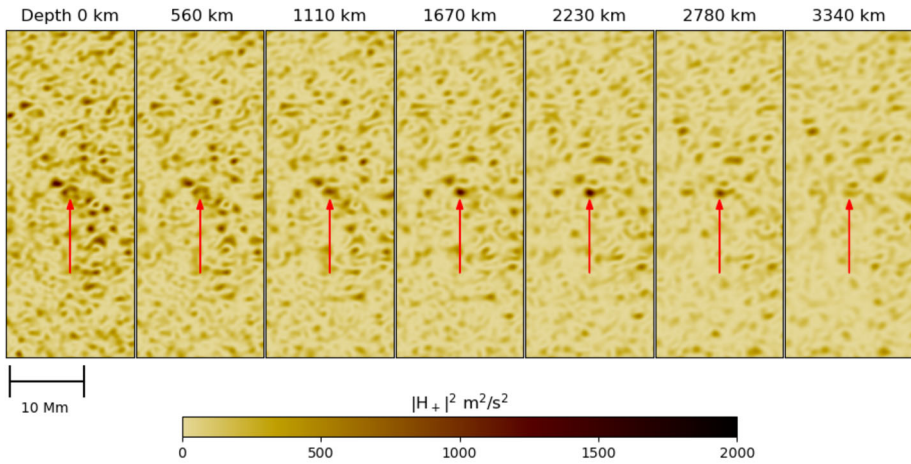
Figure 11 Sequence of acoustic source-density maps with the focal plane successively submerged from the level of the quiet photosphere (far left) to a depth of 3340 km thereunder (far right). The red arrow in each frame points to the submerged acoustic source, which comes into sharpest focus 2230 km beneath the photosphere.

Figure 12 Temporal profiles of 10-mHz source density are plotted for focal planes ranging from depth zero to 2.92 Mm. Green locus plots the source density at depth 0 Mm. Red locus plots the same at depth 2.0 Mm. The grey vertical line notes the onset of the flare, as defined by GOES. Submerged emission follows surface emission by ~ 390 s.
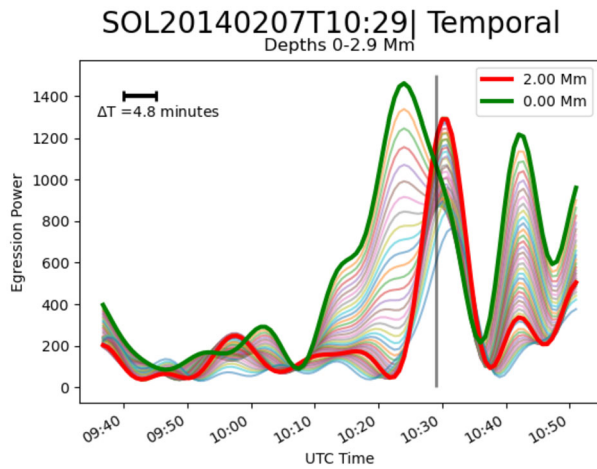
which $P_{cs}A$ condenses to 1.9×10^{-4}. It is at this location upon which the blue circles in all of the frames in Figure 10 are centered.

Figure 12 now plots the temporal profile of the $9-11$-mHz source density of the sunquake related to the flare of 2014-02-07 at 10:28 UTC integrated over a circle of radius 1.4 Mm centered on the upper circle drawn in each of the panels composing Figure 10. This is the counterpart of Figure 6 in Section 2.2, where the subject is the control case of the shallow source of emission in the flare of 2011-07-30. As in Figure 6, the sharply peaked green locus identifies the temporal profile when the focal plane is located at the surface. The red locus in the plot identifies the source profile when the focal plane is at a depth of 2.0 Mm. There appear to be two sources, a shallow one that peaks at 10:23 and a submerged one that peaks at 10:30 UTC.

Figure 13 Time-Depth map of 10-mHz source-density profiles plotted in Figure 12. The horizontal red line at depth 2.0 Mm marks our estimate of the depth of a planar dipolar source that matches the helioseismic signatures imaged in Figure 11 to within statistical uncertainties.
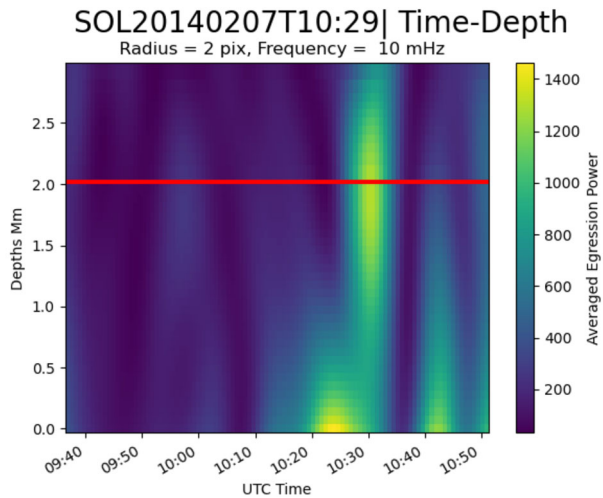
Figure 13, the counterpart of Figure 7 in Section 2.2, then renders the acoustic intensities of Figure 12 in color with vertical displacement marking focal-plane depth. The red horizontal line marks the source depth 2.0 ± 0.15 Mm that best fits the source densities imaged in Figure 11.

The 10-mHz profile of the surface source density, plotted in green in Figure 13, appears to be a sample of a confluence of several compact sources that appear in the blue circle in the lower-right frame of Figure 10. The maximum of this profile, at about 10:22 UTC, leads the onset of the X-ray and EUV emission by about six minutes. This seems to be a local Doppler precursor of the impending flare in the outer atmosphere. The significance of its submerged counterpart six minutes thence is secured largely because the background source density is so much lower in the 2-Mm submerged focal plane than at the surface. The surface signature (green locus in Figure 13) at 10:22 UTC, then, is considerably more likely to be a statistical accident than all of the nearby strong features with which it appears to be associated. This qualification should be kept in mind in the discussion that follows that proposes to associate the surface signature with its submerged counterpart. In the case of Figure 13, it also suggests that the shallow feature is distinct from the deeply submerged one, although there could be a causal connection whose acoustic signature is invisible to the helioseismic diagnostic.

3. Discussion and Conclusion

Helioseismic holography applied to HMI helioseismic observations of a sunquake that emanated from the flare of 2014-02-07 from NOAA AR11968 shows the signature of a compact acoustic source submerged to a depth of 2 Mm in the 9 – 11-mHz spectrum of the surface ripples that emanated from the flaring region. This is nearly double the depth of the ultra-impulsive source found by Martínez et al. (2020) in the flare of 2011-07-30, from NOAA AR11261. In addition to this increase in observed depth, the helioseismic source of the flare of 2014-02-07 exhibits an apparent absence of a strong shallow compact overlying source component matching the character of those apparent in the flare of 2011-07-30. This suggests that the volume of several Mm beneath active-region photospheres could possibly

harbor many more ultra-impulsive transient acoustic sources than the rarities that have so far appeared in our familiar surface-focal-plane diagnostics.

On the other hand, although the surface signature of any single surface contiguity in the bottom-right frame of Figure 10 is not very compelling by itself ($P_{cs} \sim 0.063$), there appears to be a confluence of these in the blue circle centered on the submerged source that appears in subsequent Figure 11, and these conspire to make a conspicuous surface signature in Figures 12 and 13. The separation in time between these sources is 390 s. If we propose a model in which the releases of these transients are excited by a single vertically downward propagating disturbance from the flaring outer atmosphere, then the speed of propagation comes to something like

$$v_t \sim \frac{2\,\text{Mm}}{390\,\text{s}} = 5.13\,\text{km s}^{-1}. \tag{3}$$

Lindsey et al. (2020) proposed a similar such characteristic triggering mechanism for an acoustic source 1.15 Mm beneath the quiet photosphere, leading to a downward propagating trigger at some 4.75 km s^{-1}. In both cases, the propagation speed of the trigger is decidedly less than the sound speed, but could be conformed to an Alfvén speed in a magnetic flux tube of approximately constant

$$\beta \equiv \frac{4\pi p_{\text{gas}}}{B^2}, \tag{4}$$

where B is the magnetic flux density, and p_{gas} is the gas pressure. With the statistics we have thus far, this model remains highly speculative, but not convincingly falsified in this second example we now have of submerged ultra-impulsive transient emission from a flare.

Lending additional confirmation to our measurements, we have noted a circle 100 arcseconds from the limb (Buitrago-Casas et al., 2015) on account of the distorting effects that make observation and analysis nonviable with our methods.

Finally, the foregoing developments have been heavily reinforced by the powerful control resources found in the recognition of *temporal defocusing* and its tight relationship to the standard spatial defocusing of helioseismic holography from its early advent.

Author contributions S.P.P. wrote the main manuscript text. All the authors of this manuscript participated equally in the writing and revision process.

Declarations

Competing interests The authors declare no competing interests.

References

Braun, D.C.: 1995, Scattering of *p*-modes by sunspots. I. Observations. *Astrophys. J.* **451**, 859. DOI. ADS.

Braun, D.C., Lindsey, C.: 2000, Helioseismic holography of active-region subphotospheres (invited review). *Solar Phys.* **192**, 285. DOI. ADS.

Braun, D.C., Lindsey, C., Fan, Y., Jefferies, S.M.: 1992, Local acoustic diagnostics of the solar interior. *Astrophys. J.* **392**, 739. DOI. ADS.

Braun, D.C., Lindsey, C., Fan, Y., Fagan, M.: 1998, Seismic holography of solar activity. *Astrophys. J.* **502**(2), 968. DOI. ADS.

Buitrago-Casas, J., Martínez Oliveros, J., Lindsey, C., Calvo-Mozo, B., Krucker, S., Glesener, L., Zharkov, S.: 2015, A statistical correlation of sunquakes based on their seismic and white-light emission. *Solar Phys.* **290**(11), 3151. DOI.

Cally, P.S.: 2000, Modelling *p*-mode interaction with a spreading sunspot field. *Solar Phys.* **192**, 395. DOI. ADS.

Christensen-Dalsgaard, J., Proffitt, C.R., Thompson, M.J.: 1993, Effects of diffusion on solar models and their oscillation frequencies. *Astrophys. J. Lett.* **403**, L75. DOI. ADS.

Donea, A.-C., Braun, D.C., Lindsey, C.: 1999, Seismic images of a solar flare. *Astrophys. J. Lett.* **513**(2), L143. DOI. ADS.

Donea, A.-C., Lindsey, C.: 2005, Seismic emission from the solar flares of 2003 October 28 and 29. *Astrophys. J.* **630**(2), 1168. DOI. ADS.

Donea, A.-C., Lindsey, C., Braun, D.C.: 2000, Stochastic seismic emission from acoustic glories and the quiet Sun. *Solar Phys.* **192**, 321. DOI. ADS.

Kosovichev, A., Zharkova, V.: 1998, X-ray flare sparks quake inside Sun. *Nature* **393**(6683), 317.

Lemen, J.R., Title, A.M., Akin, D.J., Boerner, P.F., Chou, C., Drake, J.F., Duncan, D.W., Edwards, C.G., Friedlaender, F.M., Heyman, G.F., Hurlburt, N.E., Katz, N.L., Kushner, G.D., Levay, M., Lindgren, R.W., Mathur, D.P., McFeaters, E.L., Mitchell, S., Rehse, R.A., Schrijver, C.J., Springer, L.A., Stern, R.A., Tarbell, T.D., Wuelser, J.-P., Wolfson, C.J., Yanari, C., Bookbinder, J.A., Cheimets, P.N., Caldwell, D., Deluca, E.E., Gates, R., Golub, L., Park, S., Podgorski, W.A., Bush, R.I., Scherrer, P.H., Gummin, M.A., Smith, P., Auker, G., Jerram, P., Pool, P., Soufli, R., Windt, D.L., Beardsley, S., Clapp, M., Lang, J., Waltham, N.: 2012, The atmospheric imaging assembly (AIA) on the solar dynamics observatory (SDO). *Solar Phys.* **275**(1–2), 17. DOI. ADS.

Lin, R.P., Dennis, B.R., Hurford, G.J., Smith, D.M., Zehnder, A., Harvey, P.R., Curtis, D.W., Pankow, D., Turin, P., Bester, M., Csillaghy, A., Lewis, M., Madden, N., van Beek, H.F., Appleby, M., Raudorf, T., McTiernan, J., Ramaty, R., Schmahl, E., Schwartz, R., Krucker, S., Abiad, R., Quinn, T., Berg, P., Hashii, M., Sterling, R., Jackson, R., Pratt, R., Campbell, R.D., Malone, D., Landis, D., Barrington-Leigh, C.P., Slassi-Sennou, S., Cork, C., Clark, D., Amato, D., Orwig, L., Boyle, R., Banks, I.S., Shirey, K., Tolbert, A.K., Zarro, D., Snow, F., Thomsen, K., Henneck, R., Mchedlishvili, A., Ming, P., Fivian, M., Jordan, J., Wanner, R., Crubb, J., Preble, J., Matranga, M., Benz, A., Hudson, H., Canfield, R.C., Holman, G.D., Crannell, C., Kosugi, T., Emslie, A.G., Vilmer, N., Brown, J.C., Johns-Krull, C., Aschwanden, M., Metcalf, T., Conway, A.: 2002, The reuven ramaty high-energy solar spectroscopic imager (RHESSI). *Solar Phys.* **210**(1), 3. DOI.

Lindsey, C., Braun, D.C.: 1997, Helioseismic holography. *Astrophys. J.* **485**(2), 895. DOI. ADS.

Lindsey, C., Braun, D.C.: 2000, Seismic images of the far side of the Sun. *Science* **287**(5459), 1799. DOI. ADS.

Lindsey, C., Buitrago-Casas, J.C., Martínez Oliveros, J.C., Braun, D., Martínez, A.D., Quintero Ortega, V., Calvo-Mozo, B., Donea, A.-C.: 2020, Submerged sources of transient acoustic emission from solar flares. *Astrophys. J.* **901**(1), L9. DOI. ADS.

Martínez, A.D., Quintero Ortega, V., Buitrago-Casas, J.C., Martínez Oliveros, J.C., Calvo-Mozo, B., Lindsey, C.: 2020, Ultra-impulsive solar flare seismology. *Astrophys. J.* **895**(1), L19. DOI. ADS.

Mumford, S.J., Freij, N., Stansby, D., Christe, S., Ireland, J., Mayer, F., Shih, A.Y., Hughitt, V.K., Ryan, D.F., Liedtke, S., Hayes, L., Pérez-Suárez, D., Vishnunarayan, K.I., Chakraborty, P., Inglis, A., Barnes, W., Pattnaik, P., Sipőcz, B., Sharma, R., Leonard, A., Hewett, R., Hamilton, A., Manhas, A., MacBride, C., Panda, A., Earnshaw, M., Choudhary, N., Kumar, A., Singh, R., Chanda, P., Haque, M.A., Kirk, M.S., Konge, S., Mueller, M., Srivastava, R., Jain, Y., Bennett, S., Baruah, A., Arbolante, Q., Charlton, M., Maloney, S., Mishra, S., Paul, J.A., Chorley, N., Chouhan, A., Himanshu, Z.L., Modi, S., Verma, A., Mason, J.P., Sharma, Y., Naman9639, Bobra, M.G., Manley, L., Rozo, J.I.C., Ivashkiv, K., Chatterjee, A., von Forstner, J.F., Stern, K.A., Bazán, J., Jain, S., Evans, J., Ghosh, S., Malocha, M., Visscher, R.D., Stańczak, D., Singh, R.R., SophieLemos, V.S., Airmansmith97, Buddhika, D., Alam, A., Pathak, H., Sharma, S., Agrawal, A., Rideout, J.R., Park, J., Bates, M., Mishra, P., Gieseler, J., Shukla, D., Taylor, G., Dacie, S., Dubey, S., Jacob, C.G., Reiter, G., Sharma, D., Inchaurrandieta, M., Goel, D., Bray, E.M., Meszaros, T., Sidhu, S., Russell, W., Surve, R., Parkhi, U., Zahniy, S., Eigenbrot, A., Robitaille, T.,

Pandey, A., Price-Whelan, A., Amogh, J., Chicrala, A., Ankit, Guennou, C., D'Avella, D., Williams, D., Verma, D., Ballew, J., Murphy, N., Lodha, P., Bose, A., Augspurger, T., Krishan, Y., honey, neerajkulk, Ranjan, K., Hill, A., Keşkek, D., Altunian, N., Bhope, A., Singaravelan, K., Kothari, Y., Molina, C., Agrawal, K., mridulpandey, Nomiya, Y., Streicher, O., Wiedemann, B.M., Mampaey, B., Agarwal, S., Gomillion, R., Gaba, A.S., Letts, J., Habib, I., Dover, F.M., Tollerud, E., Arias, E., Briseno, D.G., Bard, C., Srikanth, S., Stone, B., Jain, S., Kustov, A., Smith, A., Sinha, A., Tang, A., Kannojia, S., Mehrotra, A., Yadav, T., Paul, T., Wilkinson, T.D., Caswell, T.A., Braccia, T., yasintoda, Pereira, T.M.D., Gates, T., platipo, Dang, T.K., W, A., Bankar, V., Kaszynski, A., Wilson, A., Bahuleyan, A., Stevens, A.L., B, A., Shahdadpuri, N., Dedhia, M., Mendero, M., Cheung, M., Mangaonkar, M., Schoentgen, M., Lyes, M.M., Agrawal, Y., resakra, Ghosh, K., Hiware, K., Gyenge, N.G., Chaudhari, K., Krishna, K., Buitrago-Casas, J.C., Qing, J., Mekala, R.R., Wimbish, J., Calixto, J., Das, R., Mishra, R., Sharma, R., Babuschkin, I., Mathur, H., Kumar, G., Verstringe, F., Attie, R., Murray, S.A.: 2022, SunPy. DOI Murray, S.A.

Pesnell, W.D., Thompson, B.J., Chamberlin, P.C.: 2012, The solar dynamics observatory (SDO). *Solar Phys.* **275**(1 – 2), 3. DOI. ADS.

Roddier, F.: 1975, Principle of production of an acoustic hologram of the solar surface. *Acad. Sci. Paris C. R. Ser. B Sci. Phys.* **281**(4), 93. ADS.

Scherrer, P.H., Schou, J., Bush, R.I., Kosovichev, A.G., Bogart, R.S., Hoeksema, J.T., Liu, Y., Duvall, T.L., Zhao, J., Title, A.M., Schrijver, C.J., Tarbell, T.D., Tomczyk, S.: 2012, The helioseismic and magnetic imager (HMI) investigation for the solar dynamics observatory (SDO). *Solar Phys.* **275**(1 – 2), 207. DOI. ADS.

Schunker, H., Braun, D.C., Cally, P.S., Lindsey, C.: 2005, The local helioseismology of inclined magnetic fields and the showerglass effect. *Astrophys. J.* **621**(2), L149. DOI. ADS.

The SunPy Community, Barnes, W.T., Bobra, M.G., Christe, S.D., Freij, N., Hayes, L.A., Ireland, J., Mumford, S., Perez-Suarez, D., Ryan, D.F., Shih, A.Y., Chanda, P., Glogowski, K., Hewett, R., Hughitt, V.K., Hill, A., Hiware, K., Inglis, A., Kirk, M.S.F., Konge, S., Mason, J.P., Maloney, S.A., Murray, S.A., Panda, A., Park, J., Pereira, T.M.D., Reardon, K., Savage, S., Sipőcz, B.M., Stansby, D., Jain, Y., Taylor, G., Yadav, T., Rajul, Dang, T.K.: 2020, The SunPy project: open source development and status of the version 1.0 core package. *Astrophys. J.* **890**, 68. DOI.

Wolff, C.L.: 1972, Free oscillations of the sun and their possible stimulation by solar flares. *Astrophys. J.* **176**, 833.

Zharkov, S., Green, L.M., Matthews, S.A., Zharkova, V.V.: 2011, 2011 February 15: sunquakes produced by flux rope eruption. *Astrophys. J. Lett.* **741**(2), L35. DOI. ADS.

Zharkov, S., Green, L.M., Matthews, S.A., Zharkova, V.V.: 2013, Properties of the 15 February 2011 flare seismic sources. *Solar Phys.* **284**(2), 315. DOI. ADS.

Zharkova, V., Kosovichev, A.: 1998, Seismic response to solar flares observed SOHO/MDI. In: *Structure and Dynamics of the Interior of the Sun and Sun-Like Stars* **418**, 661.

Authors and Affiliations

Savannah Perez-Piel[1] · Juan Camilo Buitrago-Casas[1] · Juan Carlos Martínez Oliveros[1] · Charles Lindsey[2]

✉ S. Perez-Piel
savannah_sky@berkeley.edu

J.C. Buitrago-Casas
juan@berkeley.edu

J.C. Martínez Oliveros
oliveros@ssl.berkeley.edu

C. Lindsey
lindsey@nwra.com

[1] Space Sciences Laboratory, University of California Berkeley, Berkeley, CA, USA

[2] Northwest Research Associates, Boulder, CO, USA